

Topological piezoelectric response in moiré graphene systems

Ran Peng¹ and Jianpeng Liu^{1,2,*}

¹*School of Physical Science and Technology, ShanghaiTech University, Shanghai 200031, China*

²*ShanghaiTech laboratory for topological physics, ShanghaiTech University, Shanghai 200031, China*

We theoretically study the piezoelectric effects in moiré graphene systems. Since the strain couples to the electrons in the system as a pseudo vector potential, which has opposite signs for the K and K' valleys of graphene, its effects on the two valleys with opposite Chern numbers do not cancel out, but adds up. As a result, some components of the piezoelectric tensor in these systems, which typically have non-trivial topology in their flat bands, are nearly quantized in terms of the valley Chern numbers. Such a conclusion is verified by numerical calculations of the in-plane piezoelectric response of hBN-aligned twisted bilayer graphene, twisted bilayer-monolayer graphene, and twisted double bilayer graphene systems using both continuum model and atomistic tight-binding model. We find that by tuning the vertical displacement field and/or twist angle, which may induce gap closures between the flat bands and remote bands in these systems, plateau shapes of the piezoelectric response are obtained, with abrupt jumps across the topological phase transitions. We propose that such nearly quantized piezoelectric response may serve as a direct experimental probe for the valley Chern numbers of the flat bands in moiré graphene systems.

The intriguing phenomena, such as superconductivity^{1–8}, correlated insulating states^{4–7,9–14}, and quantum anomalous Hall states^{14–16}, observed in twisted bilayer graphene (TBG) around magic angle, has drawn great attention in recent years. This attention soon extends to twisted multilayer graphene systems such as twisted bilayer-monolayer graphene^{17–19} and twisted double bilayer graphene systems^{20–23}, and to hBN-graphene heterostructures^{24,25}, which exhibit equally interesting properties. All these exotic effects are believed to be attributed by the low-energy flat bands in these moiré graphene systems, which are found to be topologically non-trivial^{26–32}.

In magic-angle TBG, the low-energy states can be divided into two sets: one from the K valley, and the other from the K' valley of graphene, each of which covers the entire moiré Brillouin zone^{33,34}. Moreover, by virtue of the large moiré superlattice constant $L_s \sim 10$ nm, the intervalley scattering induced by the long-period moiré potential between the two sets of low-energy states is negligible^{33,34}, thus the total charge of each valley is approximately separately conserved characterized by valley $U(1)$ symmetry³⁵. This means that one can separately define topological quantities, such as Chern numbers^{31,32}, and Wilson loops^{27,29}, for each valley. Indeed, the nontrivial topological properties in the flat bands of magic-angle TBG are manifested as odd-winding Wilson loops^{27,29,30}, and the flat bands would acquire nonzero and valley-contrasting Chern numbers when C_{2z} symmetry is broken due to alignment of the hexagonal boron nitride (hBN) substrate^{27,28,31}. However, direct evidence of the non-trivial VCNs of the moiré graphene systems from experiments are still absent. On one hand, the expected gapless helical topological edge states from the nonzero VCNs would be gapped out by the significantly enhanced intervalley scatterings at the edges due to the atomic-scale potentials from the sample boundaries. On the other hand, without interaction-driven spontaneous valley polarization, the bands contributed by different

valleys always intertwine with their time-reversal (TR) counterpart, so that they cannot be separated by tuning the carrier density, and the topological effects from the two valleys cancel each other due to the opposite VCNs. This is true for most measures of tuning the materials, with one possible exception—strain. In low energy bands, strain does not act on the two valleys in equal way, but oppositely. A valley dependent pseudo vector potential can be induced by strain, which is opposite in the two valleys associated by TR operation. As a result, strain effect on different valleys does not cancel each other, but adds up.

The above reasoning applies to generic twisted multilayer graphene (TMG) and other moiré graphene heterostructure systems, which typically have topological flat bands with nonzero VCNs that are highly tunable by displacement fields and twist angle^{31,32,36}. Such nontrivial topological properties motivate us to study the strain effects in this whole series of systems. In the continuum model framework, we argue that the piezoelectric response of these twisted graphene systems are (nearly) quantized, in the sense that they can be expressed as a constant multiplied by the valley Chern numbers of the system. Taking hBN-aligned TBG, twisted bilayer-monolayer graphene (TBMG), and twisted double-bilayer graphene (TDBG) as examples, we have numerically calculated the piezoelectric response based on both continuum model and atomic tight-binding models, and nearly quantized plateaus of piezoelectric tensors are obtained in all of the three systems.

a. Theories of polarization and piezoelectric response — According to the modern theory of polarization^{37,38}, polarization in an insulating crystal is measured by the charge current in an adiabatic evolution that establishes the final polarized state. The theory suggests a Berry-phase-like expression for the dependence of the polariza-

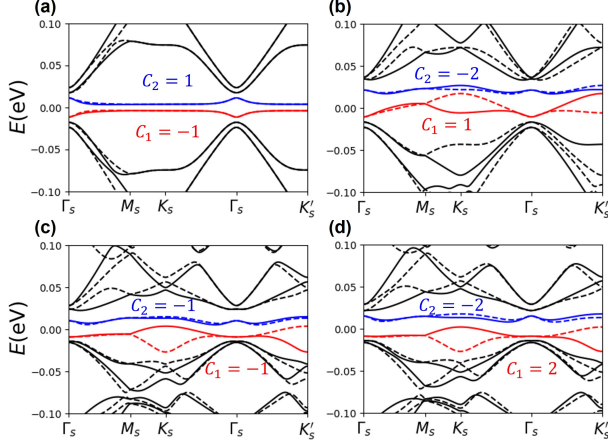


FIG. 1: Band structures of: (a) TBG with staggered sublattice potential $\Delta = 15$ meV at $\theta = 1.05^\circ$, (b) twisted bilayer-graphene with vertical electrostatic potential energy difference $U_d = -0.0536$ eV (see text) at $\theta = 1.2^\circ$, (c) AB-BA stacked TDBG with $U_d = -0.0402$ eV at $\theta = 1.2^\circ$, and (d) AB-AB stacked TDBG with $U_d = -0.0402$ eV at $\theta = 1.2^\circ$.

tion vector \mathbf{P} on the adiabatic parameter λ :

$$\frac{\partial \mathbf{P}}{\partial \lambda} = \frac{e}{(2\pi)^2} \int d^2 \mathbf{k} \sum_n \Omega_{\mathbf{k}\lambda, n}, \quad (1)$$

where

$$\Omega_{\mathbf{k}\lambda, n} = i(\langle \nabla_{\mathbf{k}} u_{n\mathbf{k}} | \partial_{\lambda} u_{n\mathbf{k}} \rangle - \langle \partial_{\lambda} u_{n\mathbf{k}} | \nabla_{\mathbf{k}} u_{n\mathbf{k}} \rangle), \quad (2)$$

and $|u_{n\mathbf{k}}\rangle$ refers to the periodic part of the n^{th} occupied Bloch function of the system. Note that Eq (2) is the correct even for a band with nonzero Chern number, although there is subtlety in considering the filling of edge states of a Chern insulator in the adiabatic process³⁹.

On the other hand, the Chern number of an isolated band $|u_{n\mathbf{k}}\rangle$ of a 2D crystal is expressed as

$$C_n = \frac{1}{2\pi i} \int d^2 \mathbf{k} (\langle \partial_{k_x} u_{n\mathbf{k}} | \partial_{k_y} u_{n\mathbf{k}} \rangle - \langle \partial_{k_y} u_{n\mathbf{k}} | \partial_{k_x} u_{n\mathbf{k}} \rangle) \quad (3)$$

The similarity between Eq. (3) and Eq. (1) indicates a possibility of topological effects to show up in 2D crystal polarization. Since strain couples to electrons as a pseudo vector potential, and the coupling coefficients have opposite signs for the opposite valleys (K and K'), we conjecture that the strain induced polarization, i.e., the piezoelectric response, may be the correct quantity to manifest nonzero VCNs of the moiré graphene systems.

The piezoelectric response is normally known as the change of polarization \mathbf{P} induced by the strain tensor μ_{jk} : $\gamma_{ijk} = \partial P_i / \partial \mu_{jk}$, which turns out to be “improper” due to possible ambiguities⁴⁰. A proper definition of piezoelectric response tensor is expressed as

$$\gamma_{ijk} = \frac{\partial \dot{P}_i}{\partial \dot{\mu}_{jk}}, \quad (4)$$

where \dot{P}_i and $\dot{\mu}_{jk}$ denote the time derivatives of the polarization and the strain, with $i, j, k = x, y$ for 2D systems. The strain tensor is defined by the shift $\Delta \mathbf{r}$ of a real-space position \mathbf{r} with respect to the original position \mathbf{r} : $\Delta r_i = \sum_{j,k=x,y} \mu_{ij} r_j$. By simply replacing the adiabatic parameter λ in Eq. (1) with strain component μ_{jk} , and multiplying both sides of Eq. (1) by $\dot{\mu}_{jk}$, we obtain the expression for the PET component contributed from the valley η ($\eta = \pm$ refers to the K and K' valleys) in the twisted graphene system:

$$\gamma_{ijk}^\eta = \frac{e}{(2\pi)^2} \int d^2 \mathbf{k} \Omega_{ijk}^\eta, \quad (5)$$

where

$$\Omega_{ijk}^\eta = \sum_n i(\langle \partial_{k_i} u_{\eta, n\mathbf{k}} | \partial_{\mu_{jk}} u_{\eta, n\mathbf{k}} \rangle - \langle \partial_{\mu_{jk}} u_{\eta, n\mathbf{k}} | \partial_{k_i} u_{\eta, n\mathbf{k}} \rangle). \quad (6)$$

Here the index n refers to the occupied band of the η valley. A small homogeneous strain applied to the system is equivalent to an effective vector potential $A_i^\eta = \xi_{ijk}^\eta \mu_{jk}$ in the η valley⁴¹, which is linearly coupled to the wavevector: $\mathbf{k} \rightarrow \mathbf{k} + \mathbf{A}^\eta$, and the partial derivative with respect to strain in Eq. (6) can be substituted by a partial derivative with respect to wavevector: $\partial_{\mu_{jk}} = \xi_{ijk}^\eta \partial_{k_i}$. As will be discussed in detail below, the prefactor ξ_{ijk}^η only depends on the properties of monolayer graphene, and is of opposite sign for the opposite valleys. Therefore, the opposite Chern numbers together with opposite strain effects means that the PET contributed by the two valleys should be the same, and is exactly quantized in terms of the VCNs of the occupied bands multiplied by a constant:

$$\gamma_{ijk} = 2(-1)^i \frac{e}{2\pi} (\xi_{ijk}^- C_- + \xi_{ijk}^+ C_+), \quad (7)$$

where C_\pm is the Chern number of the occupied bands from the K and K' valleys, and $(-1)^i = \pm 1$ for $i = x, y$. The prefactor 2 accounts for the spin degeneracy in the moiré graphene systems. The quantization of the PET can be intuitively interpreted as follows. Let us consider the situation that the strain-induced effective vector potential \mathbf{A}^η is adiabatically turned on in the system, which imposes opposite effective “electric fields” $\mathbf{E}^\eta = -\dot{\mathbf{A}}^\eta$ ($\eta = \pm$) to the two valleys, which in turn induce transverse adiabatic “Hall currents” from the two valleys with opposite Chern numbers. The adiabatic “Hall currents” generated from the two valleys are the same since both the Chern numbers and the effective electric fields are opposite for the two valleys. The piezoelectric tensor, e.g., γ_{yxx} , measures precisely the “Hall conductivity” of the adiabatic current in response to the opposite effective electric fields applied to the two valleys in the process of adiabatically turning on the strain, and such response is naturally quantized in units of VCNs of the system. In a previous work⁴², it is shown that for topologically non-trivial 2D crystalline materials with TR symmetry, a jump of piezoelectric response is expected near a topological phase transition (TPT). In the above argument, we

show that in moiré graphene systems the PET does not only exhibit discontinuity across a TPT, but are always quantized in units of the VCNs of the occupied bands no matter the system is close to a TPT or not. This is a unique property for the topologically nontrivial bands with nonzero VCNs in moiré graphene systems by virtue of the valley $U(1)$ symmetry.

b. Model Hamiltonian — To illustrate the idea of quantized PET, we first study the PET of hBN-aligned TBG based on Bistritzer-MacDonald continuum Hamiltonian³³. The effects of the hBN alignment is modeled by imposing a staggered sublattice potential $\Delta = 15$ meV to both layers, neglecting the additional moiré potential introduced by the lattice match between hBN and graphene^{28,43}, which is an order of magnitude weaker than that of TBG^{44,45}. The aligned hBN substrate breaks C_{2z} symmetry, opening a gap ~ 4 meV between the conduction and valence bands (see Fig. 1(a)), which have nonzero VCNs ± 1 . The original D_6 symmetry of the continuum model is reduced to D_3 symmetry, which requires the PET components subject to the following relation:

$$\begin{aligned}\gamma_{xxx} &= \gamma_{xyy} = \gamma_{yxy} = 0 \\ \gamma_{xxy} &= \gamma_{yxx} = -\gamma_{yyy}\end{aligned}\quad (8)$$

As a result of the D_3 symmetry, there is only one independent PET component γ_{yxx} . Note that Eq. (8) holds as long as the system has C_3 symmetry, which is present in all TMG systems. Therefore we choose to illustrate our results through the component γ_{yxx} for all twisted graphene systems discussed in this work. The Hamiltonian in the continuum model of TBG in K_η ($\eta = \mp$ represents K and K' valleys respectively) is expressed as

$$H^\eta(\mathbf{r}) = \begin{pmatrix} H_l^\eta & U_M(\mathbf{r}) \\ U_M^\dagger(\mathbf{r}) & H_2^\eta \end{pmatrix}, \quad (9)$$

where the diagonal blocks H_l^η are the monolayer layer graphene (MLG) Dirac cones at K_η valley of layer l . The off-diagonal block, which represents the interlayer coupling between the twisted bilayers introduces a moiré potential in real space $U_M(\mathbf{r})$, and the detailed expression is given in Supplementary Information⁴⁶. As mentioned in the previous section, a homogeneous strain applied to the system is equivalent to a pseudo vector potential. Here we ignore the effects of strain on the interlayer hopping⁴¹, which are considered as higher-order effects, then the strain effects are only manifested in the diagonal blocks, which become

$$H_l^\eta = \hbar v_F (\mathbf{q} + \eta \mathbf{A}_{\text{MLG}}) \cdot (\eta \sigma_x, \sigma_y) + \Delta \sigma_z, \quad (10)$$

where $\mathbf{q} = \mathbf{k} - \mathbf{K}_{l,\eta}$. For MLG in its K valley,

$$\mathbf{A}_{\text{MLG}} = -\frac{\sqrt{3}\beta}{2a}(\mu_{xx} - \mu_{yy}, -2\mu_{xy}), \quad (11)$$

where $a = 2.46 \text{ \AA}$ is the lattice constant of MLG and $\beta = 3.14$ is the decaying rate of the hopping amplitude

with respect to the distance between two carbon atoms in MLG⁴¹. This expression of strain induced vector field together with Eq. (7) tells us that in TBG system, the PET component γ_{yxx} per spin per VCN is

$$\gamma_{yxx}^0 = \frac{e}{2\pi} \frac{\sqrt{3}\beta}{2a} = -281.8 \text{ pC/m}. \quad (12)$$

Note that γ_{yxx}^0 only depends on two parameters: the graphene lattice constant a and the hopping decaying rate β , both of which are “fundamental constants” in the universe of graphene-based systems. In other words, the quantization of the PET in units of γ_{yxx}^0 remains robust regardless of the change of external tuning parameters such as external fields and twist angles.

In Fig. 2(a) we present the polarization along y direction as a function of strain u_{xx} , with twist angle $\theta = 1.05^\circ$ for hBN-aligned TBG, where the blue circles and red triangles represent the contributions from the valence and conduction flat bands with opposite Chern numbers ± 1 . Clearly the strain-induced polarizations are opposite from the two flat bands, indicating opposite PETs. In Fig. 2(b) we show the PET γ_{yxx} contributed by the valence (blue circles) and conduction (red triangles) flat bands as a function of twist angle θ . When $\theta \gtrsim 1^\circ$, the VCNs of the two flat bands are ± 1 , the calculated γ_{yxx} is around the expected quantization value $\pm 4\gamma_{yxx}^0$ (marked by the dashed lines), where the prefactor 4 is from the fourfold valley-spin degeneracy. Under the present parameter choice, when $\theta \lesssim 1^\circ$, there is a TPT due to gap closures between the flat bands and the remote bands, such that the VCNs of the flat bands become zeros. As a result, γ_{yxx} rapidly drops and becomes negligibly small as shown in Fig. 1(b). The plateau shape of γ_{yxx} - θ relationship supports our argument for the quantized PET. Fig. 2(b) also suggests a quantized jump of PET by $4\gamma_{yxx}^0$ when the carrier density is changed by ± 4 per moiré supercell with respect to the charge neutrality point.

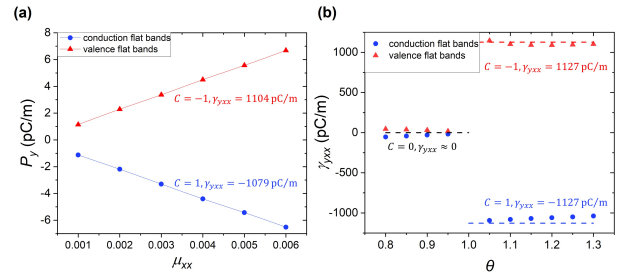


FIG. 2: (a) Plots of polarization along y direction versus strain u_{xx} for hBN-aligned TBG at $\theta = 1.05^\circ$, and (b) twist-angle (θ) dependence of γ_{yxx} contributed by the valence (red triangles) and conduction (blue dots) flat bands. The horizontal dashed lines mark the ideal quantized values.

c. PET in TMG systems — The continuum model for TBG can be readily extended to TMG systems, for

valley η , the Hamiltonian is expressed as³²

$$H_{M,\alpha;N,\alpha'}^\eta = \begin{pmatrix} H_{M,\alpha}^\eta & U \\ U^\dagger & H_{N,\alpha'}^\eta \end{pmatrix}, \quad (13)$$

where the diagonal blocks refers to $M(N)$ -layer untwisted rhombohedral graphene multilayers with stacking chiralities $\alpha(\alpha') = \pm 46^\circ$. The off-diagonal block of Eq. (B1) is an simple extension of the moiré potential in TBG in the sense that we only consider the moiré potential term between the topmost layer of the M layers and the bottom-most layer of the N layers. We refer readers to Supplementary Information for more details. The band structures for TBMG, AB-BA stacked TDBG, and AB-BA stacked TDBG calculated using the continuum model are presented in Fig. 1(b)-(d) with Chern numbers of the flat bands from the K valley being marked.

It is worthwhile to note that, with a realistic description of the system including further neighbor interlayer hoppings within each set of the untwisted multilayers⁴⁶, the strain may couple to the interlayer hopping in a similar, but slightly different way from how it couples to the intralayer hopping terms. In particular, the pseudo vector potential associated with further-neighbor interlayer hopping event is expressed as

$$\mathbf{A}_{\text{inter}} = -\lambda \frac{\sqrt{3}\beta}{2a} (\mu_{xx} - \mu_{yy}, 2\mu_{xy}) = \lambda \mathbf{A}_{\text{MLG}}, \quad (14)$$

where $\lambda = a_0/\sqrt{a_0^2 + d_{\text{AB}}^2}$, with $a_0 = a/\sqrt{3} \approx 1.42 \text{ \AA}$ and $d_{\text{AB}} = 3.35 \text{ \AA}$ being the in-plane carbon-carbon σ -bond length and the interlayer distance between AB-stacked bilayer graphene respectively. As a result of the different strain-momentum coupling terms, the substitution $\partial_{\mu_{jk}} = \xi_{ijk} \partial_{k_i}$ in deriving Eq. (7) no longer holds. Luckily, since this quantization-breaking mechanism only occurs in the further-neighbor interlayer hopping terms⁴⁶, for typical TMGs such as TBMG, and TDBG systems, the deviations of PET from the expected quantized values are very weak (see Fig. 3).

In Fig. 3, we show γ_{yxx} component as a function of twist angle θ and vertical electrostatic potential energy drop across the multilayers, denoted by U_d . Here U_d is related to the displacement field D via: $U_d = -eDd/\epsilon_{\text{hBN}}$, where $d = (M + N - 1) \times 3.35 \text{ \AA}$ is the total thickness of the twist $(M + N)$ -layer TMG system, and $\epsilon_{\text{hBN}} \approx 5$ is the dielectric constant of the hBN substrate, *e.g.*, $D = 0.1 \text{ V/nm}$ corresponds to $U_d = -0.0134 (M + N - 1) \text{ eV}$. As suggested by Ref.³², in the chiral limit, the total VCNs of the two flat bands per spin equals to ± 1 for TBMG and ± 2 for AB-BA stacked TDBG. This conclusion conforms to the calculated values of γ_{yxx} and VCNs in the largest plateau of each subplot of Fig. 3. As the further neighbor interlayer hoppings and external displacement fields break the chiral limit, the total VCNs of the two flat bands change as a function U_d and θ , as shown in Fig. 3(c) and (d) for TBMG and TDBG respectively, hence making the PETs jump to different quantized plateaus as shown in Fig. 3(a) and (b). The calculated PETs and VCNs agree with each other very well.

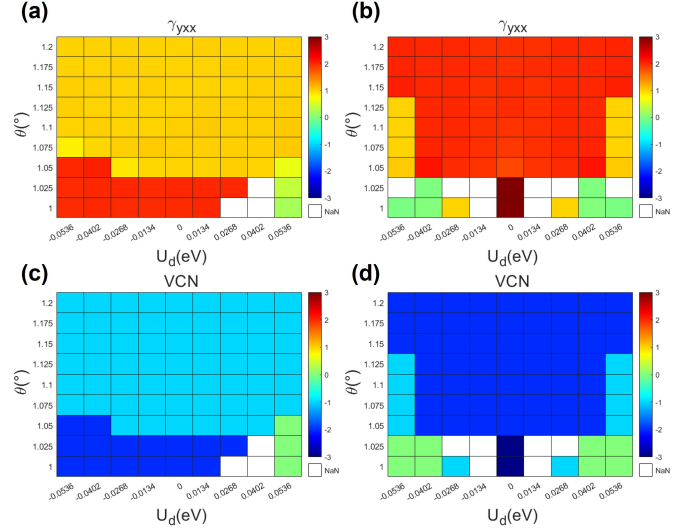


FIG. 3: PET and VCNs of all flat bands in TBMG and TDBG systems: (a) γ_{yxx} of TBMG as a function of θ and U_d ; (b) γ_{yxx} of AB-BA stacked TDBG as a function of θ and U_d ; (c) Total Chern numbers of the two flat bands from K valley of TBMG as a function of θ and U_d ; (d) Total Chern numbers of the two flat bands from K valley of AB-BA stacked TDBG as a function of θ and U_d . In Fig. (a) and (b), the values of γ_{yxx} are shown in the units of $|4\gamma_{yxx}^0| = 1127 \text{ pC/m}$. The blank patches indicate points which are too close to gap closures such that VCNs are ill defined.

As the flat bands are reported to be isolated from the remote bands for these TMG systems^{17,18,20–23,47}, we suggest that PET contributed by the flat bands can be extracted in experiments by comparing the PETs with filling factor $+4$ and -4 , *i.e.*, when the flat bands are fully occupied or empty. By tuning the vertical displacement field, the PET contributed by the flat bands would remain stable and nearly constant, until the field is strong enough to drive a TPT, with a quantized jump of PET. In this way, the VCNs of the flat bands of the TMG systems can be directly detected by measuring the piezoelectric response.

The above argument of quantized PET is based on two approximations: (i) the K and K' valleys are decoupled, which is an excellent approximation for moiré graphene systems and is widely adopted in literatures, and (ii) the effects of homogeneous strain on the moiré potentials have been neglected, which deserves further verification. We have further checked the validity of approximation (ii) by directly calculating the piezoelectric response of hBN-aligned TBG and TBMG based on a realistic atomistic Slater-Koster tight-binding model adopted from Ref.⁴⁸, which can include all the strain effects on the electronic structures. For hBN-aligned TBG, our results indicate that γ_{yxx} *vs.* θ plot still exhibits a plateau shape with an abrupt jump at $\theta \approx 1^\circ$ due to a TPT (VCNs become zeros for $\theta \lesssim 1^\circ$) although the quantization is not quite exact due to the strain effects on the moiré potential, with $\gamma_{yxx} \approx \pm 1.2 \times 4\gamma_{yxx}^0$ when the VCNs are ± 1 .

for $\theta \gtrsim 1^\circ$ ⁴⁶. We have also calculated the U_d dependence of γ_{yxx} in TBMG contributed by the two flat bands at $\theta = 1.25^\circ$, and find a plateau of $\gamma_{yxx} \approx 1.15 \times 4\gamma_{yxx}^0$ ⁴⁶, compatible with the total VCN ± 1 .

In this work we apply the modern polarization theory for crystals to the case of piezoelectric response in moiré graphene systems, and suggest a possible way of measuring the VCNs in these systems based on piezoelectric response. We propose that for moiré graphene systems with valley charge conservation, the PET is exactly quantized as integer multiples of the VCNs under certain mild approximations. Although this quantization is not exact in a more realistic situation, it turns out that the quantization condition is only slightly deviated, so that the plateau patterns of the PET are still clearly present for typical twisted graphene systems such as hBN-aligned TBG, TBGM, and TDBG systems. By tuning external displacement fields and twist angle, which can affect the topological properties of the flat bands in the TMG systems, the PET plateaus can be directly measured by experiments, which manifest the VCNs of the flat bands.

Acknowledgments

This work is supported by the National Key R & D program of China (grant no. 2020YFA0309601), the National Science Foundation of China (grant no. 12174257), and the start-up grant of ShanghaiTech University. We would like to thank Prof. Yue Zhao for valuable discussions.

Appendix A: Continuum model of twisted bilayer graphene systems

To introduce the continuum model of moiré graphene systems^{32,33}, we first start with twisted bilayer graphene (TBG). The general idea of continuum model is to express the low energy Hamiltonian H^η of TBG in the basis of MLG Bloch states. As shown in Fig. 4, the moiré Brillouin zone (mBZ) of TBG is much smaller than the MLG Brillouin zone for small twist angle θ . As a result, by choosing a mBZ that is near the $K(K')$ valley of MLG, the intralayer part of TBG Hamiltonian can be well approximated by the Dirac cone form of the MLG Hamiltonian:

$$\langle \mathbf{k}_l, X_l | H^\eta | \mathbf{k}_l, X'_l \rangle = (H_l^\eta)_{X_l X'_l},$$

$$H_l^\eta = \hbar v_F R(-\theta_l) (\mathbf{q}_l + \eta \mathbf{A}_{\text{MLG}}) \cdot (\eta \sigma_x, \sigma_y), \quad (\text{A1})$$

where $\eta = \pm$ refers to $K(K')$ valley, $\mathbf{q}_l = \mathbf{k}_l - \mathbf{K}_{l,\eta}$ is the momentum relative to the K_η valley of layer l , $X_l, X'_l = A_l, B_l$ refers to the A, B sublattices of each layer, and \mathbf{A}_{MLG} is the strain induced vector potential (see main text). If strain and staggered sublattice potential are included, as in main text, we should add an extra mass term $\Delta\sigma_z$ to the second equation of Eq. (A1) (see main

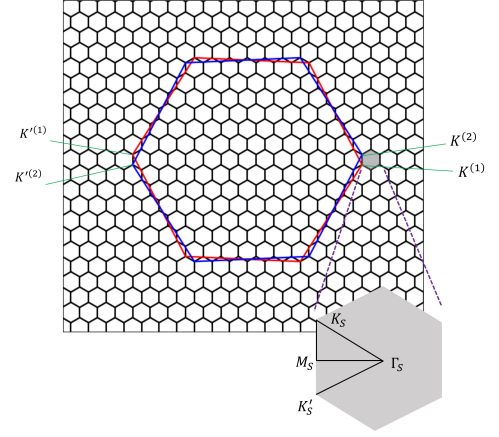


FIG. 4: A plot of the Brillouin zones of the two layers of monolayer graphene (MLG) (where layer 1 is marked with red color and layer 2 is marked with blue color) and the moiré Brillouin zone (mBZ) of TBG (each hexagonal patch of the lattice). The inset zooms in a moiré Brillouin zone and the high symmetry path used in Fig. 1 of the main text is marked. The twist angle in the plot ($\sim 5^\circ$) is larger than the ones in main text for clarity.

text). Since the twist angles are generally very small in such systems, we can take the rotational operation $R(\theta_l)$ to be identity. We choose $\hbar v_F/a = 2.1354 \text{ eV}$ as in Ref. (49), where $a = 2.46 \text{ \AA}$ is the lattice constant of MLG.

To consider the interlayer part of H^η , we start with an untwisted AA stacked bilayer graphene. The two layers are then twisted by $\theta_l = (-1)^l \theta/2$ around a common A sublattice site. The general form of an interlayer term for hopping from layer 2 to layer 1 is

$$\langle \mathbf{k}_1, X_1 | H^\eta | \mathbf{k}_2, X_2 \rangle = \frac{1}{\sqrt{N_1 N_2}} \sum_{\mathbf{R}_1, \mathbf{R}_2} e^{-i\mathbf{k}_1 \cdot (\mathbf{R}_1 + \boldsymbol{\tau}_1, X_1)} \times t_{12}^{X_1 X_2}(\mathbf{R}_1, \mathbf{R}_2) e^{i\mathbf{k}_2 \cdot (\mathbf{R}_2 + \boldsymbol{\tau}_2, X_2)}, \quad (\text{A2})$$

where \mathbf{R}_l are the lattice points of the two layers, and $t_{12}^{X_1 X_2} = t(\mathbf{R}_1 + \boldsymbol{\tau}_1, X_1 - \mathbf{R}_2 - \boldsymbol{\tau}_2, X_2)$ is the hopping amplitude between two atomic orbitals, which has the Slater-Koster form⁴⁸:

$$t(\mathbf{R}) = V_{pp\pi} [1 - (\frac{\mathbf{R} \cdot \mathbf{e}_z}{R})^2] + V_{pp\sigma} (\frac{\mathbf{R} \cdot \mathbf{e}_z}{R})^2,$$

$$V_{pp\pi} = V_{pp\pi}^0 e^{-(R-a_0)/r_0}, \quad V_{pp\sigma} = V_{pp\sigma}^0 e^{-(R-d_0)/r_0}, \quad (\text{A3})$$

where $a_0 = a/\sqrt{3}$ is the in-plane carbon-carbon sigma bond length, and $d_0 = d_{\text{AB}} = 3.35 \text{ \AA}$ is the interlayer distance between AB-stacked bilayer graphene. The parameters in Eq. (A3) are chosen to be: $V_{pp\pi}^0 = -2.7 \text{ eV}$, $V_{pp\sigma}^0 = 0.48 \text{ eV}$, and $r_0 = 0.184a$ so as to fit the hopping within MLG and between AB-stacked bilayer graphene. Note that for in-plane hopping, Eq. (A3) is reduced to

$$t(R) = V_{pp\pi}^0 e^{-\beta(R/a_0-1)}, \quad (\text{A4})$$

where $\beta = a_0/r_0 = 3.14$ is the decaying rate that appears in the strain induced vector field in graphene (see main text). By Fourier transforming the hopping amplitude in Eq. (A2), the interlayer hopping term finally becomes (see more details in Ref. 48,50)

$$\langle \mathbf{k}_1, X_1 | H^\eta | \mathbf{k}_2, X_2 \rangle = \frac{1}{S_M} \int_{S_M} d^2\mathbf{r} (U_M)_{X_1 X_2} e^{i(\mathbf{k}_1 - \mathbf{k}_2) \cdot \mathbf{r}}. \quad (\text{A5})$$

The Hamiltonian H^η now can be written under the basis $|A_1\rangle, |B_1\rangle, |A_2\rangle, |B_2\rangle$ as

$$H^\eta(\mathbf{r}) = \begin{pmatrix} H_1^\eta & U_M(\mathbf{r}) \\ U_M^\dagger(\mathbf{r}) & H_2^\eta \end{pmatrix}, \quad (\text{A6})$$

where

$$U_M(\mathbf{r}) = \begin{pmatrix} u & u' \\ u' & u \end{pmatrix} + \begin{pmatrix} u & u'\omega^{-\eta} \\ u'\omega^\eta & u \end{pmatrix} e^{i\eta \mathbf{G}_2^M \cdot \mathbf{r}} + \begin{pmatrix} u & u'\omega^\eta \\ u'\omega^{-\eta} & u \end{pmatrix} e^{-i\eta \mathbf{G}_1^M \cdot \mathbf{r}}, \quad (\text{A7})$$

with $\omega = e^{i2\pi/3}$, $\mathbf{G}_1^M = 4\pi/(\sqrt{3}L_s)(1/2, -\sqrt{3}/2)$, $\mathbf{G}_2^M = 4\pi/(\sqrt{3}L_s)(1/2, \sqrt{3}/2)$ being the Moiré reciprocal basis vectors, and L_s being the moiré supercell lattice constant. The parameters are chosen to be $u = 0.0797$ eV, $u' = 0.0975$ eV, and the difference between u and u' characterizes the corrugation of TBG⁵⁰, whose main effect is to separate the flat bands from the others. The derivation of Eq. (A7) is the same as in Ref. 48, except for a different choice of basis vectors and sublattices.

Appendix B: Continuum model of twisted multilayer graphene systems

The continuum model of TBG constructed above can be easily extended to twisted multilayer graphene (TMG) systems. The Hamiltonian of an $(M + N)$ -layer TMG system with stacking chiralities $\alpha, \alpha' = \pm$ is expressed as

$$H_{M,\alpha;N,\alpha'}^\eta = \begin{pmatrix} H_{M,\alpha}^\eta & U \\ U^\dagger & H_{N,\alpha'}^\eta \end{pmatrix}, \quad (\text{B1})$$

where a diagonal block, *e.g.*, for the bottom M layers and positive stacking chirality, is

$$H_{M,+}^\eta = \begin{pmatrix} H_1^\eta & U_{AB} & 0 & 0 & \cdots \\ U_{AB}^\dagger & H_1^\eta & U_{AB} & 0 & \cdots \\ 0 & U_{AB}^\dagger & H_1^\eta & U_{AB} & \cdots \\ \vdots & \vdots & \vdots & \vdots & \ddots \end{pmatrix}. \quad (\text{B2})$$

In Eq. (B2), the diagonal blocks, *i.e.*, the intralayer Hamiltonian, are the same as the one defined in Eq. (A1), except that $\Delta = 0$ here; and matrix U_{AB} refers to the interlayer hopping between AB stacking bilayer graphene, with

$$U_{AB} = \begin{pmatrix} 0 & 0 \\ t_1 & 0 \end{pmatrix}, \quad (\text{B3})$$

where $t_1 = 0.48$ eV is the hopping amplitude between two atoms in different layers with the same horizontal position. If the stacking chirality is reversed in Eq. (B2), we may simply replace U_{AB} with $U_{BA} = U_{AB}^\dagger$. The off-diagonal block of Eq. (B1) is

$$U = \begin{pmatrix} 0 & 0 & \cdots & 0 \\ 0 & 0 & \cdots & 0 \\ \vdots & \vdots & \ddots & \vdots \\ U_M & 0 & \cdots & 0 \end{pmatrix}, \quad (\text{B4})$$

where the only non-zero block refers to the interlayer coupling between the bottom layer of the upper N layers and the top layer of the bottom M layers, which has the same definition as Eq. (A7). As discussed in main text, the moiré graphene systems should show quantized piezoelectric response as long as the strain linearly couples to the momentum, which is the case of Eq. (A1). Under the approximation where the effects by strain to interlayer hopping are ignored, piezoelectricity contributed by low energy bands of TBG is quantized. We can see that under the current model Hamiltonian for TMG, strain still enters the Hamiltonian by linearly coupling to the momentum through vector potential \mathbf{A}_{MLG} because Eq. (B3) is independent of strain. Therefore, our argument for quantized piezoelectric response in TBG is also valid for the TMG systems.

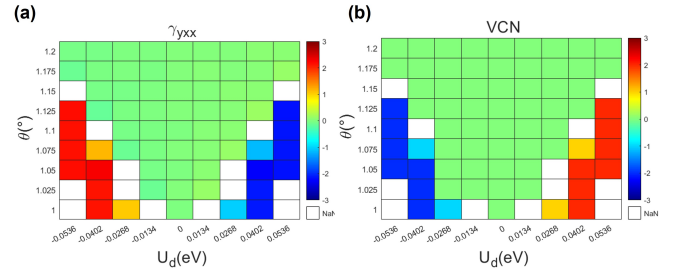


FIG. 5: A plot of (a) the γ_{yxx} component of PET and (b) the VCN from K valley of AB-AB stacked TDBG as a function of twist angle θ and vertical electrostatic potential energy drop U_d across the multilayers.

However, In our numerical calculation, we adopt a more realistic version of the interlayer hopping between untwisted layers:

$$U_{AB} = \begin{pmatrix} t_2 f(\mathbf{k}) & t_2 f^*(\mathbf{k}) \\ t_1 - t_3 & t_2 f(\mathbf{k}) \end{pmatrix}, \quad (\text{B5})$$

where $t_2 = 0.21$ eV and $t_3 = 0.05$ eV are the second and third nearest interlayer hopping amplitude, and $f(\mathbf{k}) = -(\sqrt{3}a/2)(\eta q_x - i q_y)$ for momenta near the K_η valley. Here

$$(q_x, q_y) = \mathbf{k} - \mathbf{K}_{l,\eta} + \eta \mathbf{A}_{\text{inter}}, \quad (\text{B6})$$

with $\mathbf{A}_{\text{inter}} = \lambda \mathbf{A}_{\text{MLG}}$, $\lambda = a_0 / \sqrt{a_0^2 + d_{\text{AB}}^2}$, as shown in main text. Now the untwisted interlayer hopping and intralayer hopping couple to the strain in different ways with further-neighbor interlayer hopping, so the piezoelectric response quantization is no longer conserved. Luckily, this quantization breaking mechanism is weak, as is shown by the results in main text. In this part, we also show piezoelectric tensor (PET) of AB-AB stacked twisted double bilayer graphene (TDBG), which is not shown in the main text because in the major area of the parameter space, the valley Chern number (VCN) of all flat bands equal to zero³², and thus the PET by the two flat bands (per spin per valley) are hard to be measured.

Appendix C: Tight-binding model

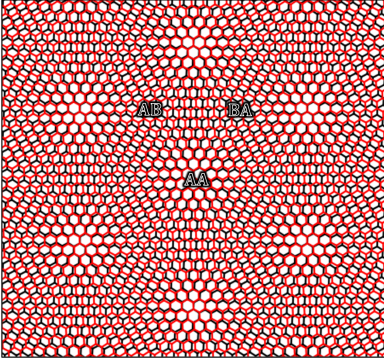


FIG. 6: A plot of the real space moiré pattern in TDBG, where the AB, BA, and AA zones are marked.

To check the validity of the results based on continuum model, we also implemented atomistic tight-binding model based calculations, which are computationally more demanding, but provide more reliable results. To construct the tight-binding model Hamiltonian, we need to describe the positions of the carbon atoms in a moiré supercell. We start with AA stacked bilayer graphene, where the positions of the atoms in layer l ($l = 1, 2$) at sublattice α ($\alpha = A, N$) are given by

$$\begin{aligned} \mathbf{R}_{l,\alpha}^{mn} &= (\mathbf{R}_{l,\alpha}^{mn})_{\parallel} + \mathbf{d}_{l,\alpha}^{mn}, \\ (\mathbf{R}_{l,\alpha}^{mn})_{\parallel} &= m\mathbf{a}_1 + n\mathbf{a}_2 + \boldsymbol{\tau}_{\alpha}, \end{aligned} \quad (\text{C1})$$

with $\mathbf{a}_1, \mathbf{a}_2$ being the real space basis vectors of graphene, $\boldsymbol{\tau}_{\alpha}$ being the position of a sublattice relative to the graphene unit cell, and $\mathbf{d}_{l,\alpha}^{mn} = (-1)^l d[(\mathbf{R}_{l,\alpha}^{mn})_{\parallel}] / 2 \mathbf{e}_z$ being the vertical displacement of two aligned atoms. After the two layers are twisted by $\theta_l = (-1)^l \theta / 2$, the positions of the atoms become $\mathbf{R}_{l,\alpha}^{mn}(\theta_l) = R(\theta_l) \mathbf{R}_{l,\alpha}^{mn}$. As shown in Fig. 6, the TDBG is divided into AB and AA stacked zones, which share the same period with the moiré supercell. As a result, the interlayer distances are different in these zones, *i.e.*, TDBG is corrugated. The corrugation

can be interpolated by the following function⁵⁰:

$$d_{l,\alpha}^{mn} = d_0 + 2d_1 \sum_{i=1}^3 \cos \mathbf{b}_i \boldsymbol{\delta}[(\mathbf{R}_{l,\alpha}^{mn})_{\parallel}], \quad (\text{C2})$$

where $\mathbf{b}_1 = (2\pi/(\sqrt{3}a), 2\pi/a)$, $\mathbf{b}_2 = (2\pi/(\sqrt{3}a), -2\pi/a)$ are the reciprocal basis vectors of MLG, and $\mathbf{b}_3 = -\mathbf{b}_1 - \mathbf{b}_2$. The function $\boldsymbol{\delta}$ is defined as $\boldsymbol{\delta}(\mathbf{R}) = [R(\theta_2) - R(\theta_1)] \mathbf{R}$, which refers to the displacement of two aligned atoms in AA stacked bilayer graphene after twisted. In a commensurate structure of TBG, once \mathbf{R} is changed by a moiré lattice vector, $\boldsymbol{\delta}(\mathbf{R})$ is changed by an MLG lattice vector, so Eq. (C2) shares the same period as the moiré superlattice. To fit the interlayer distances of $d_{\text{AB}} = 3.35 \text{ \AA}$ and $d_{\text{AA}} = 3.60 \text{ \AA}$ ^{51,52}, the parameters are chosen to be $d_0 = (d_{\text{AA}} + 2d_{\text{AB}})/3$ and $d_1 = (d_{\text{AA}} - d_{\text{AB}})/9$.

Once the positions of the atoms in the supercell are determined, it is straight-forward to derive the tight-binding model Hamiltonian with the hopping amplitudes between each pair of atomic orbitals given by Eq. (A3). The Hamiltonian under the Bloch basis of TBG is

$$H = \sum_{\mathbf{k}, \mathbf{R}} \sum_{i,j} t(\mathbf{R} + \boldsymbol{\tau}_i - \boldsymbol{\tau}_j) e^{i\mathbf{k}(\mathbf{R} + \boldsymbol{\tau}_i - \boldsymbol{\tau}_j)} |\mathbf{k}, i\rangle \langle \mathbf{k}, j|, \quad (\text{C3})$$

where \mathbf{R} refers to the moiré lattice vectors, and i, j represent the sublattices in moiré supercell.

In Fig. (7), we show the calculated γ_{yxx} component of PET based on the above atomistic tight-binding model. In particular, in Fig. (7)(a) we show the twist angle dependence of γ_{yxx} for hBN-aligned TBG, where the blue circles and red triangles represent γ_{yxx} contributed by the valence flat band and conduction flat band with opposite valley Chern numbers ± 1 . Clearly we see a plateau shape of γ_{yxx} as a function of θ , with an abrupt drop when $\theta \lesssim 1^\circ$. This is because with our choice of parameters, there is an topological phase transition with gap closures between the flat bands and the remote bands, such that the valley Chern numbers of the flat bands become zeros when $\theta \lesssim 1^\circ$. When the valence chern numbers are ± 1 , we see that $\gamma_{yxx} \approx \pm 1.2 \times (4\gamma_{yxx}^0)$, which are mildly deviated from the expected quantized value $\pm 4\gamma_{yxx}^0$. However, the plateau shape is well preserved, indicating the topological nature of the piezoelectric response. In Fig. 7(b) we show the calculated γ_{yxx} as a function of vertical electrostatic potential drop U_d , contributed by the 8 flat bands (including valley and spin degrees of freedom) in AB-A stacked twisted bilayer-monolayer graphene system with $\theta = 1.25^\circ$. The total valley Chern number of the two flat bands per spin per valley remains as ± 1 for $-0.03 \text{ eV} \leq U_d \leq 0.03 \text{ eV}$, thus we expect to see a plateau of γ_{yxx} with quantized value of $\pm 4\gamma_{yxx}^0$. The calculated $\gamma_{yxx} \approx \pm 1.15 \times (4\gamma_{yxx}^0)$, which still exhibits a plateau shape. The deviations to the expected quantized value are attributed to the strain effects on the moiré potentials, which are neglected in continuum model, but captured in the atomistic tight-binding model.

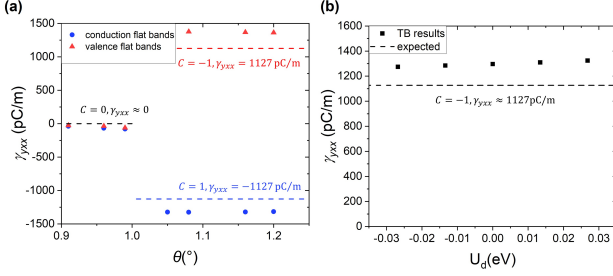


FIG. 7: Tight-binding model based results for PET component γ_{yxx} of (a) hBN-aligned TBG, contributed by the conduction (blue dots) and valence (red triangles) flat bands, as functions of twist angle θ ; and (b) AB-A stacked TMG, contributed by all the flat bands, as a function of vertical electrostatic potential energy drop U_d . In both (a) and (b), the predicted values of γ_{yxx} for the corresponding bands given by $4\gamma_{yxx}^0 = -1127\text{pC/m}$ per VCN are marked by the dashed lines.

Appendix D: Derivation of the vector field induced by strain

We start with the MLG Hamiltonian without approximations:

$$H_{\text{MLG}} = \begin{pmatrix} 0 & g(\mathbf{k}, \hat{\mu}) \\ g^*(\mathbf{k}, \hat{\mu}) & 0 \end{pmatrix}, \quad (\text{D1})$$

where $g(\mathbf{k}, \hat{\mu}) = \sum_{i=1}^3 t_0^{(i)} e^{i\mathbf{k} \cdot \mathbf{r}_i}$, with $t_0^{(i)} = t(|\mathbf{r}_i|)$ being the nearest-neighbor hopping amplitude of graphene, $\mathbf{r}_1, \mathbf{r}_2, \mathbf{r}_3$ being the nearest-neighbor hopping vectors of graphene, and $t(\mathbf{R})$ being the Slater-Koster form defined in Eq. (A4). When the system is free of strain, $\mathbf{r}_1^0 = (0, a_0)$, $\mathbf{r}_2^0 = a_0(\sqrt{3}/2, -1/2)$, $\mathbf{r}_3^0 = a_0(-\sqrt{3}/2, -1/2)$. Under presence of strain $\hat{\mu}$, which has the form of

$$\hat{\mu} = \begin{pmatrix} \mu_{xx} & \mu_{xy} \\ \mu_{xy} & \mu_{yy} \end{pmatrix}, \quad (\text{D2})$$

each vector \mathbf{r}_i undergoes small shifts from \mathbf{r}_i^0 to $(1 + \hat{\mu})\mathbf{r}_i^0$, which leads to a change $\delta t^{(i)} = t(\mathbf{r}_i) - t(\mathbf{r}_i^0)$ in the hopping amplitudes, *e.g.*,

$$\begin{aligned} \delta t(\mathbf{r}_1) &\approx -t_0\beta\mu_{yy}, \\ \delta t(\mathbf{r}_2) &\approx -t_0\beta\left(\frac{3}{4}\mu_{xx} - \frac{\sqrt{3}}{2}\mu_{xy} + \frac{1}{4}\mu_{yy}\right), \\ \delta t(\mathbf{r}_3) &\approx -t_0\beta\left(\frac{3}{4}\mu_{xx} + \frac{\sqrt{3}}{2}\mu_{xy} + \frac{1}{4}\mu_{yy}\right), \end{aligned} \quad (\text{D3})$$

where $t_0 = t(\mathbf{r}_i^0)$ is the unstrained nearest-neighbor hopping amplitude. By expanding $g(\mathbf{k})$ near the K_η valleys, with $\mathbf{K}_\eta = \eta(4\pi/(3a), 0)$, we have

$$g(\mathbf{q}, \hat{\mu}) = g(\mathbf{q}, 0) + \delta g(\mathbf{q}, \hat{\mu}), \quad (\text{D4})$$

where $\mathbf{q} = \mathbf{k} - \mathbf{K}_\eta$, and $g(\mathbf{q}, 0)$ is the off-diagonal component of unstrained Dirac cone:

$$g(\mathbf{q}, 0) = \hbar v_F(\eta q_x - i q_y), \quad (\text{D5})$$

and

$$\delta g(\mathbf{q}, \hat{\mu}) = -\beta t_0 \left[\left(\frac{3}{4}\mu_{xx} - \frac{3}{4}\mu_{yy} \right) + i\eta \frac{3}{2}\mu_{xy} \right]. \quad (\text{D6})$$

So the expression of $g(\mathbf{q}, \hat{\mu})$ can finally be written as

$$g(\mathbf{q}, \hat{\mu}) = \hbar v_F [\eta(q_x + \eta A_{\text{MLG}}^x) - i(q_y + \eta A_{\text{MLG}}^y)], \quad (\text{D7})$$

or, equivalently,

$$g(\mathbf{q}, \hat{\mu}) = g(\mathbf{q} + \eta \mathbf{A}_{\text{MLG}}, 0), \quad (\text{D8})$$

with

$$A_{\text{MLG}}^x = -\frac{\sqrt{3}\beta}{2a}(\mu_{xx} - \mu_{yy}), \quad A_{\text{MLG}}^y = -\frac{\sqrt{3}\beta}{a}\mu_{xy}. \quad (\text{D9})$$

From Eq. (D8) we can see that the effects by strain near the K_η valleys of graphene is equivalent to a vector potential.

The strain induced vector field $\mathbf{A}_{\text{inter}}$ (see text) for the further-neighbor hopping between AB stacked bilayers can be derived in similar way, except that the strain only changes the horizontal components of the interlayer carbon-carbon displacement vector. As a result, their distance is changed in a lower rate, and so is the hopping amplitude, which leads to a constant factor $\lambda = a_0/\sqrt{a_0^2 + d_{\text{AB}}^2} < 1$ to the corresponding vector potential.

* liujp@shanghaitech.edu.cn

¹ Y. Cao, V. Fatemi, S. Fang, K. Watanabe, T. Taniguchi, E. Kaxiras, and P. Jarillo-Herrero, *Nature* **556**, 43 (2018).

² M. Yankowitz, S. Chen, H. Polshyn, Y. Zhang, K. Watanabe, T. Taniguchi, D. Graf, A. F. Young, and C. R. Dean, *Science* **363**, 1059 (2019).

³ E. Codecido, Q. Wang, R. Koester, S. Che, H. Tian, R. Lv, S. Tran, K. Watanabe, T. Taniguchi, F. Zhang, et al., *Science Advances* **5** (2019).

⁴ X. Lu, P. Stepanov, W. Yang, M. Xie, M. A. Aamir, I. Das, C. Urgell, K. Watanabe, T. Taniguchi, G. Zhang, et al., *Nature* **574**, 653 (2019).

⁵ P. Stepanov, I. Das, X. Lu, A. Fahimniya, K. Watanabe, T. Taniguchi, F. H. L. Koppens, J. Lischner, L. Levitov, and D. K. Efetov, *Nature* **583**, 375 (2020), ISSN 1476-4687.

⁶ Y. Saito, J. Ge, K. Watanabe, T. Taniguchi, and A. F.

- Young, *Nature Physics* **16**, 926 (2020), ISSN 1745-2481.
- ⁷ X. Liu, Z. Wang, K. Watanabe, T. Taniguchi, O. Vafek, and J. Li, *Science* **371**, 1261 (2021).
 - ⁸ Y. Cao, D. Rodan-Legrain, J. M. Park, N. F. Yuan, K. Watanabe, T. Taniguchi, R. M. Fernandes, L. Fu, and P. Jarillo-Herrero, *science* **372**, 264 (2021).
 - ⁹ Y. Cao, V. Fatemi, A. Demir, S. Fang, S. L. Tomarken, J. Y. Luo, J. D. Sanchez-Yamagishi, K. Watanabe, T. Taniguchi, E. Kaxiras, et al., *Nature* **556**, 80 (2018).
 - ¹⁰ A. Kerelsky, L. J. McGilly, D. M. Kennes, L. Xian, M. Yankowitz, S. Chen, K. Watanabe, T. Taniguchi, J. Hone, C. Dean, et al., *Nature* **572**, 95 (2019).
 - ¹¹ Y. Jiang, X. Lai, K. Watanabe, T. Taniguchi, K. Haule, J. Mao, and E. Y. Andrei, *Nature (London)* **573**, 91 (2019).
 - ¹² Y. Xie, B. Lian, B. Jäck, X. Liu, C.-L. Chiu, K. Watanabe, T. Taniguchi, B. A. Bernevig, and A. Yazdani, *Nature (London)* **572**, 101 (2019).
 - ¹³ Y. Choi, J. Kemmer, Y. Peng, A. Thomson, H. Arora, R. Polski, Y. Zhang, H. Ren, J. Alicea, G. Refael, et al., *Nature Physics* pp. 1–7 (2019).
 - ¹⁴ M. Serlin, C. Tschirhart, H. Polshyn, Y. Zhang, J. Zhu, K. Watanabe, T. Taniguchi, L. Balents, and A. Young, *Science* (2019).
 - ¹⁵ A. L. Sharpe, E. J. Fox, A. W. Barnard, J. Finney, K. Watanabe, T. Taniguchi, M. A. Kastner, and D. Goldhaber-Gordon, *Science* **365**, 605 (2019).
 - ¹⁶ P. Stepanov, M. Xie, T. Taniguchi, K. Watanabe, X. Lu, A. H. MacDonald, B. A. Bernevig, and D. K. Efetov (2020), 2012.15126.
 - ¹⁷ H. Polshyn, J. Zhu, M. Kumar, Y. Zhang, F. Yang, C. Tschirhart, M. Serlin, K. Watanabe, T. Taniguchi, A. MacDonald, et al., *Nature* pp. 1–5 (2020).
 - ¹⁸ S. Chen, M. He, Y.-H. Zhang, V. Hsieh, Z. Fei, K. Watanabe, T. Taniguchi, D. H. Cobden, X. Xu, C. R. Dean, et al., *Nat. Phys.* (2020).
 - ¹⁹ S. Xu, M. M. Al Ezzi, N. Balakrishnan, A. Garcia-Ruiz, B. Tsim, C. Mullan, J. Barrier, N. Xin, B. A. Piot, T. Taniguchi, et al., *Nature Physics* (2021), ISSN 1745-2481.
 - ²⁰ X. Liu, Z. Hao, E. Khalaf, J. Y. Lee, Y. Ronen, H. Yoo, D. Haei Najafabadi, K. Watanabe, T. Taniguchi, A. Vishwanath, et al., *Nature* **583**, 221 (2020).
 - ²¹ C. Shen, Y. Chu, Q. Wu, N. Li, S. Wang, Y. Zhao, J. Tang, J. Liu, J. Tian, K. Watanabe, et al., *Nature Physics* **16**, 520 (2020), ISSN 1745-2481.
 - ²² Y. Cao, D. Rodan-Legrain, O. Rubies-Bigorda, J. M. Park, K. Watanabe, T. Taniguchi, and P. Jarillo-Herrero, *Nature* (2020), ISSN 1476-4687.
 - ²³ C. Rubio-Verdú, S. Turkel, L. Song, L. Klebl, R. Samajdar, M. S. Scheurer, J. W. F. Venderbos, K. Watanabe, T. Taniguchi, H. Ochoa, et al., *arXiv preprint arXiv:2009.11645* (2020).
 - ²⁴ G. Chen, A. L. Sharpe, P. Gallagher, I. T. Rosen, E. J. Fox, L. Jiang, B. Lyu, H. Li, K. Watanabe, T. Taniguchi, et al., *Nature* **572**, 215 (2019), ISSN 1476-4687.
 - ²⁵ G. Chen, L. Jiang, S. Wu, B. Lyu, H. Li, B. L. Chittari, K. Watanabe, T. Taniguchi, Z. Shi, J. Jung, et al., *Nat. Phys.* **15**, 237 (2019).
 - ²⁶ H. C. Po, L. Zou, T. Senthil, and A. Vishwanath, *Phys. Rev. B* **99**, 195455 (2019).
 - ²⁷ J. Liu, J. Liu, and X. Dai, *Phys. Rev. B* **99**, 155415 (2019).
 - ²⁸ N. Bultinck, S. Chatterjee, and M. P. Zaletel, *Phys. Rev. Lett.* **124**, 166601 (2020).
 - ²⁹ Z. Song, Z. Wang, W. Shi, G. Li, C. Fang, and B. A. Bernevig, *Phys. Rev. Lett.* **123**, 036401 (2019).
 - ³⁰ J. Ahn, S. Park, and B.-J. Yang, *Phys. Rev. X* **9**, 021013 (2019).
 - ³¹ Y.-H. Zhang, D. Mao, and T. Senthil, *Phys. Rev. Research* **1**, 033126 (2019).
 - ³² J. Liu, Z. Ma, J. Gao, and X. Dai, *Phys. Rev. X* **9**, 031021 (2019).
 - ³³ R. Bistritzer and A. H. MacDonald, *Proceedings of the National Academy of Sciences* **108**, 12233 (2011).
 - ³⁴ J. M. B. Lopes dos Santos, N. M. R. Peres, and A. H. Castro Neto, *Phys. Rev. B* **86**, 155449 (2012).
 - ³⁵ H. C. Po, L. Zou, A. Vishwanath, and T. Senthil, *Phys. Rev. X* **8**, 031089 (2018).
 - ³⁶ M. Koshino, *Phys. Rev. B* **99**, 235406 (2019).
 - ³⁷ R. King-Smith and D. Vanderbilt, *Phys. Rev. B* **47**, 1651 (1993).
 - ³⁸ R. Resta and D. Vanderbilt, in *Physics of Ferroelectrics: a Modern Perspective*, edited by K. M. Rabe, C. H. Ahn, and J.-M. Triscone (Springer-Verlag, Berlin, 2007).
 - ³⁹ S. Coh and D. Vanderbilt, *Phys. Rev. Lett.* **102**, 107603 (2009).
 - ⁴⁰ D. Vanderbilt, *Journal of Physics and Chemistry of Solids* **61**, 147 (2000), ISSN 0022-3697.
 - ⁴¹ Z. Bi, N. F. Q. Yuan, and L. Fu, *Phys. Rev. B* **100**, 035448 (2019).
 - ⁴² J. Yu and C. Liu, *Nature communications* **11**, 2290 (2020).
 - ⁴³ Y.-H. Zhang, D. Mao, and T. Senthil, *Phys. Rev. Research* **1**, 033126 (2019).
 - ⁴⁴ P. Moon and M. Koshino, *Phys. Rev. B* **90**, 155406 (2014).
 - ⁴⁵ J. Jung, A. Raoux, Z. Qiao, and A. H. MacDonald, *Phys. Rev. B* **89**, 205414 (2014).
 - ⁴⁶ See Appendix for: (a) the detailed presentation of the continuum models for the twisted bilayer, and twisted multilayer graphene systems; (b) the results of piezoelectric response from atomistic tight-binding calculations; and (c) the derivations for the strain induced vector fields in graphene;.
 - ⁴⁷ M. He, Y. Li, J. Cai, Y. Liu, K. Watanabe, T. Taniguchi, X. Xu, and M. Yankowitz, *Nat. Phys.* (2020).
 - ⁴⁸ P. Moon and M. Koshino, *Physical Review B* **87**, 205404 (2013).
 - ⁴⁹ N. Marzari and D. Vanderbilt, *Phys. Rev. B* **56**, 12847 (1997).
 - ⁵⁰ M. Koshino, N. F. Q. Yuan, T. Koretsune, M. Ochi, K. Kuroki, and L. Fu, *Phys. Rev. X* **8**, 031087 (2018).
 - ⁵¹ J.-K. Lee, S.-C. Lee, J.-P. Ahn, S.-C. Kim, J. I. Wilson, and P. John, *The Journal of chemical physics* **129**, 234709 (2008).
 - ⁵² K. Uchida, S. Furuya, J.-I. Iwata, and A. Oshiyama, *Phys. Rev. B* **90**, 155451 (2014).